Distinct impact of substrate hydrophilicity on performance and structure of TFC NF and RO polyamide membranes

Ruobin Dai,[†] Zhe Yang,[‡] Zhiwei Qiu,[†] Li Long,[‡] Chuyang Y. Tang,[*,‡] and Zhiwei Wang[*,†]

[†] State Key Laboratory of Pollution Control and Resource Reuse, Shanghai Institute of Pollution Control and Ecological Security, Tongji Advanced Membrane Technology Center, School of Environmental Science and Engineering, Tongji University, Shanghai 200092, China

[‡] Department of Civil Engineering, the University of Hong Kong, Pokfulam Road, Hong Kong S.A.R., China

[*] Corresponding authors:

tangc@hku.hk (C. Tang);

zwwang@tongji.edu.cn (Z. Wang).

Abstract

Substrate properties have profound impacts on the structure and performance of both thin-film composite (TFC) nanofiltration (NF) and reverse osmosis (RO) polyamide (PA) membranes. Some studies have previously investigated the impact of substrate hydrophilicity on PA formation and TFC membrane performance. However, the observed phenomena and explanations remain contradictory in literature. Herein, we performed interfacial polymerization (IP) reactions of both piperazine (PIP)-trimesoyl chloride (TMC) and m-phenylenediamine (MPD)-TMC systems on substrates with different hydrophilicity. We found that the TFC RO membrane showed higher water permeance and NaCl rejection on the relatively hydrophobic substrate, while the TFC NF membrane favored the relatively hydrophilic substrate. The critical importance of interfacial degassing and local monomer concentration was highlighted to dissect the distinct impact of substrate hydrophilicity. For the MPD-TMC system, interfacial nanobubble generation was inhibited because of the decreased local MPD concentration and heat production for the more hydrophilic substrates, resulting in a decrease in the roughness feature and compromised water permeance of RO membranes. In contrast, interfacial degassing was not a dominant mechanism in the PIP-TMC system due to the slower reaction rate of PIP-TMC than MPD-TMC. Consequently, the PA layer of NF membrane became thinner and looser when the substrate became more hydrophilic, resulting from the diluted local PIP concentration. Our study unveils the fundamental relationship among substrate hydrophilicity, PA structure, and separation performance of both TFC NF and RO PA membranes, providing important guides on their design and synthesis.

Keywords: hydrophilicity; substrate; thin-film composite; nanofiltration; reverse osmosis

1. Introduction

Nanofiltration (NF) and reverse osmosis (RO) technologies play crucial roles in desalination, wastewater treatment, and water reuse[1–3], to address the global challenge of water scarcity and environmental pollution[4–6]. To make these technologies more energetically efficient, intensive efforts have been dedicated to developing NF and RO membranes with both high water permeance and selectivity[7–9]. Prevailing NF and RO membranes are typically formulated in a thin-film composite (TFC) structure based on polyamide (PA) chemistry[10–12]. To prepare NF or RO membranes, an amine monomer aqueous solution of piperazine (PIP) or m-phenylenediamine (MPD) is first used for wetting a porous substrate, and a trimesoyl chloride (TMC) organic solution is then applied to initiate the interfacial polymerization (IP), resulting in the formation of a continuous, thin, and cross-linked PA active layer[11]. The structure of the PA nanofilm is highly correlated with the separation performance of TFC NF or RO membrane[13,14]. RO membranes often show PA structural feature of "ridge-and-valley" (or leaf-like structure) containing numerous nanosized voids, which are beneficial for fast water transport[14,15]. In contrast, NF membranes typically possess PA nanofilms with nodular structures, though stripe-like structure has been also explored for improving the effective filtration area and increasing water permeance[7,13,16].

The structure of PA nanofilm is strongly affected by the substrate properties[17–19]. One of the most important features of the substrate is the hydrophilicity, which has a vital impact on the structure of PA nanofilm for both NF and RO membranes[18–20]. Nevertheless, the exact role of substrate hydrophilicity remains controversial in literature. Ghosh and Hoek[19] proposed that hydrophobic polysulfone (PSf) substrate could favor the convex meniscus in the pores and the amine ejection, resulting in the rougher PA structure and improved water permeability for the RO membrane, whereas using hydrophilic substrates may lead to less permeable TFC membranes[19,21]. In contrast, some researchers noticed that hydrophilic pores would allow favorable storage of amine solution, benefiting the sufficient supply of amine monomer during the IP reaction and leading to more permeable PA layers[18,22]. Moreover, hydrophilic interlayer modifications on relatively hydrophobic substrates were reported to act as the amine reservoir and facilitate the synthesis of highly permeable PA NF membranes[10,23,24]. These apparent conflicts call for a systematic and in-depth exploration to unravel the underlying mechanisms dominating the impact of substrate hydrophilicity on the structure and performance of TFC NF and RO membranes.

We hypothesize that the affinity and sorption behavior of monomers (MPD or PIP) and water onto the substrates with varied hydrophilicity could be different, possibly resulting in a contrasting local monomer concentration on the substrates and thereby different IP conditions. Recent studies have demonstrated that the amine availability plays an important role in polyamide morphology and performance [25,26]. Moreover, recent advances in the PA formation mechanism may also provide useful clues for dissecting the role of substrate hydrophilicity. Ma et al.[27,28] unraveled that the generation of acid and heat during the IP would induce interfacial degassing, converting the bicarbonate in the MPD solution into CO_2 nanobubbles at the interface. Those nanobubbles, encapsulated between PA nanofilm and substrates, were proven responsible for the leaf-like feature of the PA layer for TFC RO membranes[11,14,29,30]. In contrast, for PIP-TMC system typically used for TFC NF membrane fabrication, the production of nanobubbles at the interface could be markedly diminished due to the decreased production of H^+ and heat at the interface, resulting from the slower reaction rate of PIP-TMC than that of MPD-TMC system[31,32]. The discrepancy in nanobubble generation conditions for PIP-TMC and MPD-TMC systems may cause a difference in the response of PA structure to the same substrate.

Herein, we performed IP reactions of both PIP-TMC and MPD-TMC systems on substrates with different hydrophilicity, to reveal the distinct impact of substrate hydrophilicity on the performance and structure of TFC NF and RO PA membranes. We found that the TFC RO membrane showed higher water permeance and NaCl rejection on the relatively hydrophobic substrate, while the TFC NF membrane favored the relatively hydrophilic substrate. The critical importance of interfacial degassing and local monomer concentration was highlighted to dissect the distinct impact of substrate hydrophilicity. Our study unveils the fundamental relationship among substrate hydrophilicity, PA structure, and separation performance of TFC PA membranes, providing guides on the design and synthesis of both NF and RO membranes.

2. Materials and Methods

2.1. Preparation of substrates with varied hydrophilicity

The preparation method of PSf ultrafiltration substrates was modified from our previous study[24]. Polyvinylpyrrolidone (PVP) powder was used for adjusting the hydrophilicity of PSf substrates. Briefly, PSf beads (15 wt%) and PVP powders (0, 2, 4, 6 wt%) were dissolved in N, N-dimethylformamide (DMF) and continuously stirred for 24 h at 25°C. After degassing, the solution was directly casted on a clean glass plate by a casting knife (Elcometer, UK), with a height of 150 μm. The glass plate after casting was directly subject to phase inversion in a deionized (DI) water bath. The obtained PSf substrates were rinsed and conserved in DI water overnight before further use or characterization. The PSf substrates with different PVP contents (0, 2, 4, 6 wt% in DMF) were denoted as PVP0, PVP2, PVP4, and PVP6, respectively. To compensate the possible effect of PVP addition on substrate pore size, we prepared another group of PSf substrate with higher PSf concentration (18 wt% in DMF) and 6 wt% PVP (labeled as PVP6+) as an additional control.

2.2. Fabrication of TFC NF and RO membranes

PIP and MPD were used as the aqueous monomers for the fabrication of TFC NF and RO membranes, respectively. The PSf substrates with varied hydrophilicity were first immersed in an aqueous solution of PIP or MPD (2.0 wt/v%) for 2 min. After squeezing by a rubber roller, the surfaces of PSf substrates were exposed to TMC/hexane (0.15 wt/v%) for 1 min reaction of IP. The resulting TFC membranes were rinsed by hexane and subsequently water, and then stored in DI water overnight for further use or characterization.

2.3. Membrane characterization

The morphological features of the surface of substrates and TFC membranes were observed by a field-emission scanning electron microscope (FESEM, Hitachi S-4800). The membrane coupons were coated with Pt and Au after being oven-dried at 40°C. The acceleration voltage for SEM observation was 5.0 kV. Average pore sizes of different PSf substrates were determined by Nano Measurer 1.2 software from the SEM images. In detail, membrane area of 20 μm^2 and approximately 400 pores were analyzed for each sample, and two replicate samples of each membrane type were analyzed. The error bars are the standard error of all the pores across the different replicates analyzed. Cross-sectional transmission electron microscopy characterization (TEM, FEI Tecnai G2) was carried out to observe the cross-sectional images of the TFC membranes based on a previous study[33]. Atomic force microscopy (AFM), attenuated total reflectance-Fourier transform infrared spectroscopy (ATR-FTIR), X-ray photoelectron spectroscopy (XPS), zeta potential, and water contact angle measurements of the substrates or membranes were documented in our previous works[34,35].

2.4. Membrane Performance Evaluation

Membrane separation performance including water flux and solute rejection for TFC NF and RO membranes was tested using laboratory-scale cross-flow filtration systems. NF and RO membranes were pre-compacted at 5.0 and 17.0 bar for 2 h at 25°C, and tested at 4.0 and 15.5 bar for performance evaluation, respectively. A pre-compaction pressure higher than the testing pressure can enable more efficient stabilization of the membrane performance. The water flux (J_v) and water permeance (A) were calculated by Eqs. (1) and (2).

$$J_\mathrm{v} = \frac{\Delta m}{\Delta t \times a \times \rho} \tag{1}$$

$$A = \frac{J_\mathrm{v}}{\Delta P - \Delta \pi} \tag{2}$$

in which Δm represents the permeate mass during a given time interval (Δt), a represents the effective area for membrane filtration, ρ represents the water density, ΔP represents the applied pressure, and $\Delta \pi$ represents the osmotic pressure difference across the membrane. The solute rejection (R) and solute permeability (B) were calculated based on Eqs. (3) and (4).

$$R = \frac{C_\mathrm{f} - C_\mathrm{p}}{C_\mathrm{f}} \times 100\% \tag{3}$$

$$B = \left(\frac{1}{R} - 1 \right) \times J_\mathrm{v} \tag{4}$$

in which C_f and C_p represent concentrations of solute in the feed and permeate, respectively.

Na_2SO_4 and NaCl were used for evaluating salt rejections of NF and RO membranes, respectively. The concentrations of Na_2SO_4 and NaCl in the feed were 1000 mg/L and 2000 mg/L, respectively. A total organic carbon analyzer (TOC-L, SHIMADZU) was used to determine the concentrations of neutral solutes (dextrose and 1,4-dioxane). The concentrations of neutral solutes were 40 mg/L in TOC.

2.5. Molecular Docking

Molecular docking was performed based on the AutoDock Vina program to quantify the interaction force between PSf and PIP/MPD/water. The geometrical structures of polysulfone ($n = 5$), PIP, MPD and water molecules were built and optimized by ChemDraw software. These molecules were then processed by adding Gasteiger-Hücker empirical charge, combining nonpolar hydrogen as well as setting rotatable bonds via AutoDockTools software. The 140×140×140 Å docking square boxes were set at the central sites of polysulfone ($n = 5$) through AutoDock Vina program. Finally, the conformational search and energy optimization of PIP, MPD, and water molecules was carried out in these boxes, respectively. The calculation processing was terminated after obtaining the best binding conformations of each molecule pair.

2.6. Uptake of Monomer and Aqueous Solution by Substrates

The uptake of PIP/water solution or MPD/water solution by various PSf substrates was quantified by the weight change after wetting by 2.0 wt/v % PIP/water or MPD/water for 2 min. The PSf substrates saturated with PIP/water or MPD/water were then subject to drying in a 40°C oven and characterized by XPS for determining nitrogen content on the surfaces of substrates. The surfaces of substrates without monomer sorption were also characterized by XPS since the PVP additives also contain nitrogen elements, which need to be subtracted. The

PIP or MPD sorption (without water) by various substrates was thereby quantified according to the difference between the nitrogen contents. The quantification of PIP or MPD sorption by substrates was carried out in triplicate.

3. Results and Discussion

3.1. Characterization of different substrates with varied hydrophilicity

Morphological observation using SEM (Fig. 1A) shows the typical structure of UF membranes for five PSf substrates[36]. The presence of PVP in PVP2, PVP4, PVP6, and PVP6+ substrates was validated by ATR-FTIR spectra (Fig. 1B), in which the characteristic peak of 1670 cm^{-1} relating to -C=O stretching vibration was intensified after dosing PVP[37,38]. A slight increase in surface average pore size was noticed for PVP0-PVP6 substrates after addition of PVP (Fig. 1C, Fig. S1). As expected, the water contact angles decreased with the increase of PVP dosage for PVP0-PVP6 substrates (Fig. 1D) due to the hydrophilic nature of PVP additive [39], while the PVP6+ substrate possessed a larger water contact angle than that of the PVP6 substrate, resulting from the increased dosage of relatively hydrophobic PSf.

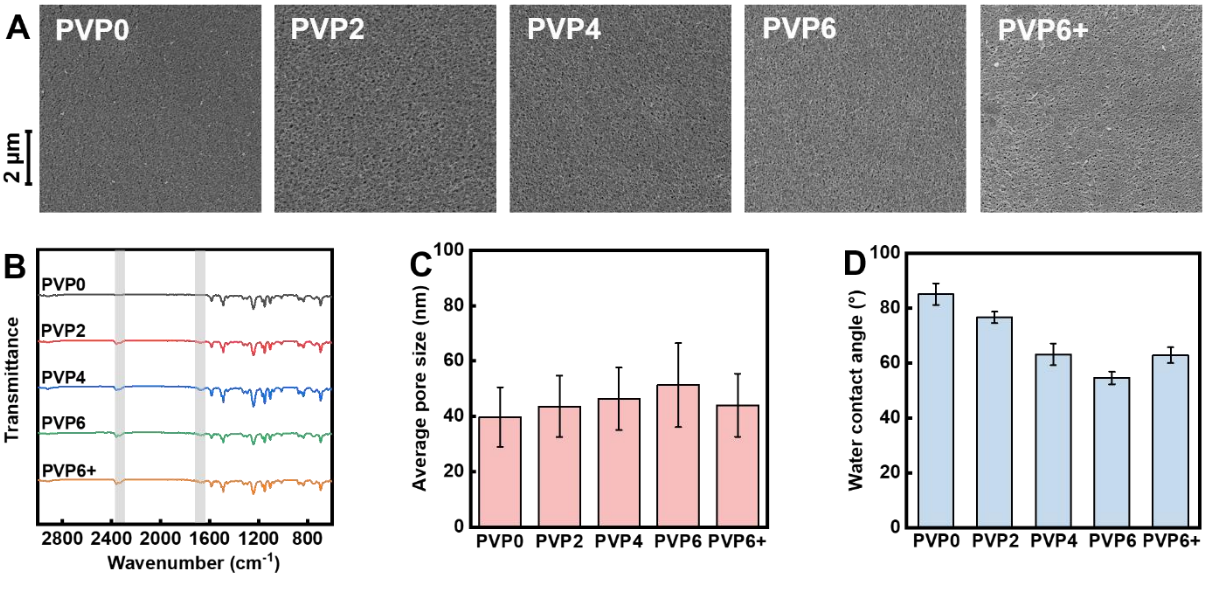

Fig. 1. Characterization of different ultrafiltration PSf substrates. (A) Surface morphologies of various PSf substrates characterized by SEM. (B) ATR-FTIR spectra of different PSf substrates with a wavenumber range of 600 – 3000 cm^{-1}. (C) Average pore sizes of different PSf substrates, which were determined by Nano Measurer 1.2 software from the SEM images; (D) Water contact angles of surfaces of different substrates. The reported water contact angles are the average values of seven independent measurements.

3.2. Performance of TFC NF and RO Membranes Fabricated on Different Substrates

IP reactions of PIP-TMC and MPD-TMC systems were conducted for the fabrication of TFC NF and RO membranes on the substrates with varied hydrophilicity, respectively. Water permeance of the TFC NF membrane increased markedly with an increase in substrate hydrophilicity (Fig. 2A). For example, the water permeance of NF-PVP0 membrane was 8.8 ± 1.2 L m^{-2} h^{-1} bar^{-1}, while the value was more than doubled for the NF-PVP6 membrane. Simultaneously, Na_2SO_4 rejection of various NF membranes was nearly identical (>97%). Recent studies suggested that hydrophilic interlayer-based modification on hydrophobic substrates can distinctly increase the water permeance of formed NF membranes[10,23,24]. Although the gutter effect was claimed to be largely responsible for the enhanced water permeance[23,24], the effect of more hydrophilic reaction platform could also contribute to the possibly tailored PA structure and subsequently the increased water permeance for TFC NF membranes.

Surprisingly, the TFC RO membranes showed a contrasting tendency in water permeance to the TFC NF membranes on the substrates (Fig. 2B), *i.e.*, hydrophobic substrates produced higher water permeance for RO membranes (*e.g.*, 2.9 ± 0.2 L m^{-2} h^{-1} bar^{-1} for RO-PVP0 membrane) than those of relatively hydrophilic substrates (*e.g.*, 1.2 ± 0.1 L m^{-2} h^{-1} bar^{-1} for RO-PVP6 membrane). Although this observation appears to be counterintuitive, they are consistent with previous studies[19,20,40]. Moreover, the RO membranes prepared on hydrophilic substrates showed compromised NaCl rejections (*e.g.*, NaCl rejection rate of 94.9 ± 2.3% for RO-PVP6 membrane) compared with that of hydrophobic substrates (*e.g.*, 98.4 ± 0.3% for RO-PVP0 membrane). Rejection of neutral solute of 1,4-dioxane (88 Da) showed similar tendency to the rejection of NaCl by RO membranes (Fig. 2C), indicative of a weakened size exclusion effect[41]. Despite an increase in the negative charge of the surface of RO membranes prepared on hydrophilic substrates (Fig. S2), it seems that the increased electrostatic repulsion between Cl^- and the membrane surface cannot compensate for the weakened size exclusion effect.

In contrast, although rejection of neutral solute (dextrose, 180 Da) and surface zeta potential of the NF membranes showed the same response to the substrates as those of the RO membranes, the Na_2SO_4 rejection of NF membranes was not compromised when hydrophilicity of corresponding substrates increased. This phenomenon can be explained by the stronger electrostatic repulsion of divalent SO_4^{2-} with membrane surface and its larger radius of hydrated ion over monovalent Cl^- ion. Fig. 2D indicates that the cross-linking degrees of both NF and RO membranes decreased with the increase in hydrophilicity of substrates, verifying their looser PA structures with weakened size exclusion effects and more negatively charged surfaces.

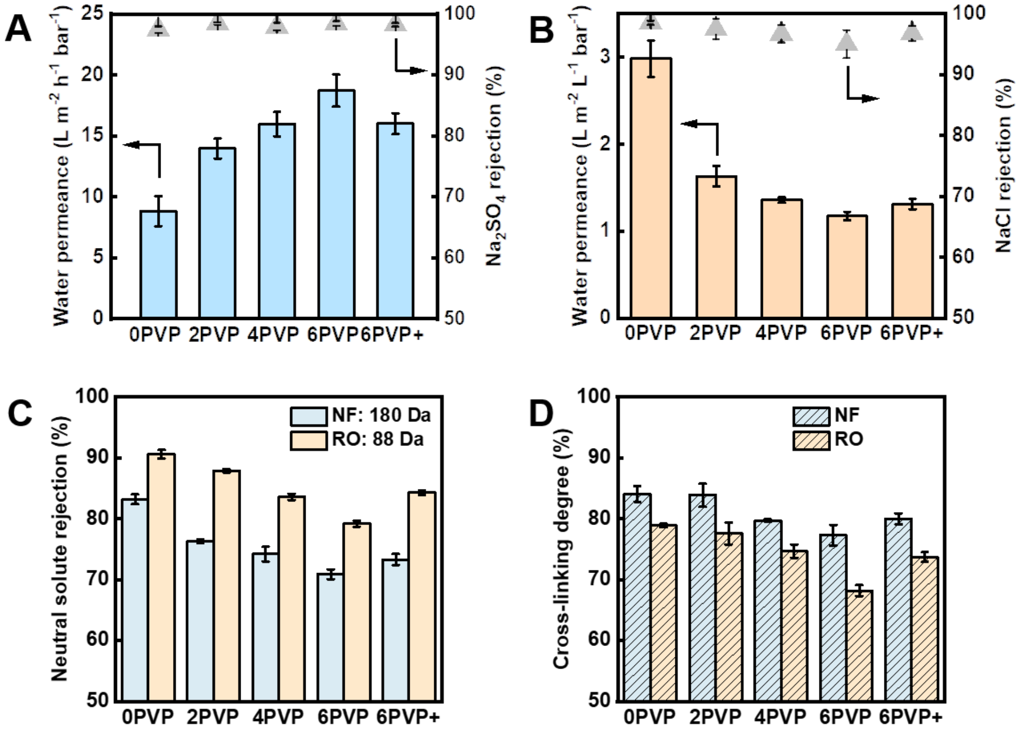

Fig. 2. Performance and polyamide cross-linking degrees of various TFC NF and RO membranes synthesized on different PSf substrates. (A) Water permeance and Na_2SO_4 rejection of NF membranes fabricated on different substrates. The concentration of Na_2SO_4 was 1000 mg/L and the feed temperature was 25°C. (B) Water permeance and NaCl rejection of RO membranes fabricated on different substrates. The concentration of NaCl was 2000 mg/L and the feed temperature was 25°C. (C) Neutral solute rejection of NF and RO membranes fabricated on different substrates. Neutral solutes of dextrose (180 Da) and 1,4-dioxane (88 Da) were used to probe the size exclusion effect of NF and RO membranes, respectively. The concentration of neutral solute was 40 mg/L in terms of total organic carbon, while the feed temperature was 25°C. (D) Cross-linking degrees of PA active layers of NF and RO membranes. The cross-linking degrees were calculated based on XPS spectra of surfaces of corresponding membranes.

3.3. Morphological characterization

The change in the structure of PA layers has a vital impact on water permeance and solute rejection of NF and RO membranes[10,42,43]. No obvious change in the structure of PA layers of the NF membranes was noticed from projected SEM images, cross-sectional TEM images, and AFM topographies (Figs. 3A, B and Fig. S3). The surfaces of RO membranes showed leaf-like (or ridge and valley) roughness features and the RO-PVP0 membrane had the most significant ridge and valley morphologies. Enhancing the substrate hydrophilicity (from PVP0 to PVP6) resulted in the diminishing of those leaf-like features (Figs. 3C, D and Fig. S4). The leaf-like structures were formed because of the interfacial degassing of CO_2 nanobubbles[27,30] which were constrained between the polyamide film and substrate. Due to the generation of acid and heat during the IP, the dissolved bicarbonate will be degassed[27]. Enlarging the pore size of the substrate could alleviate the confinement effect [30] but it should not be the major reason for the diminishing of leaf-like structures in this study, since the pore size of substrates only had slight difference (Fig. 1C). The confinement effect refers to the phenomenon that the substrate pores can restrict the downward escape of nanobubbles, and hence a stronger confinement effect results in more nanobubbles constrained between PA layer and substrate, thereby beneficial for shaping roughened PA structure.

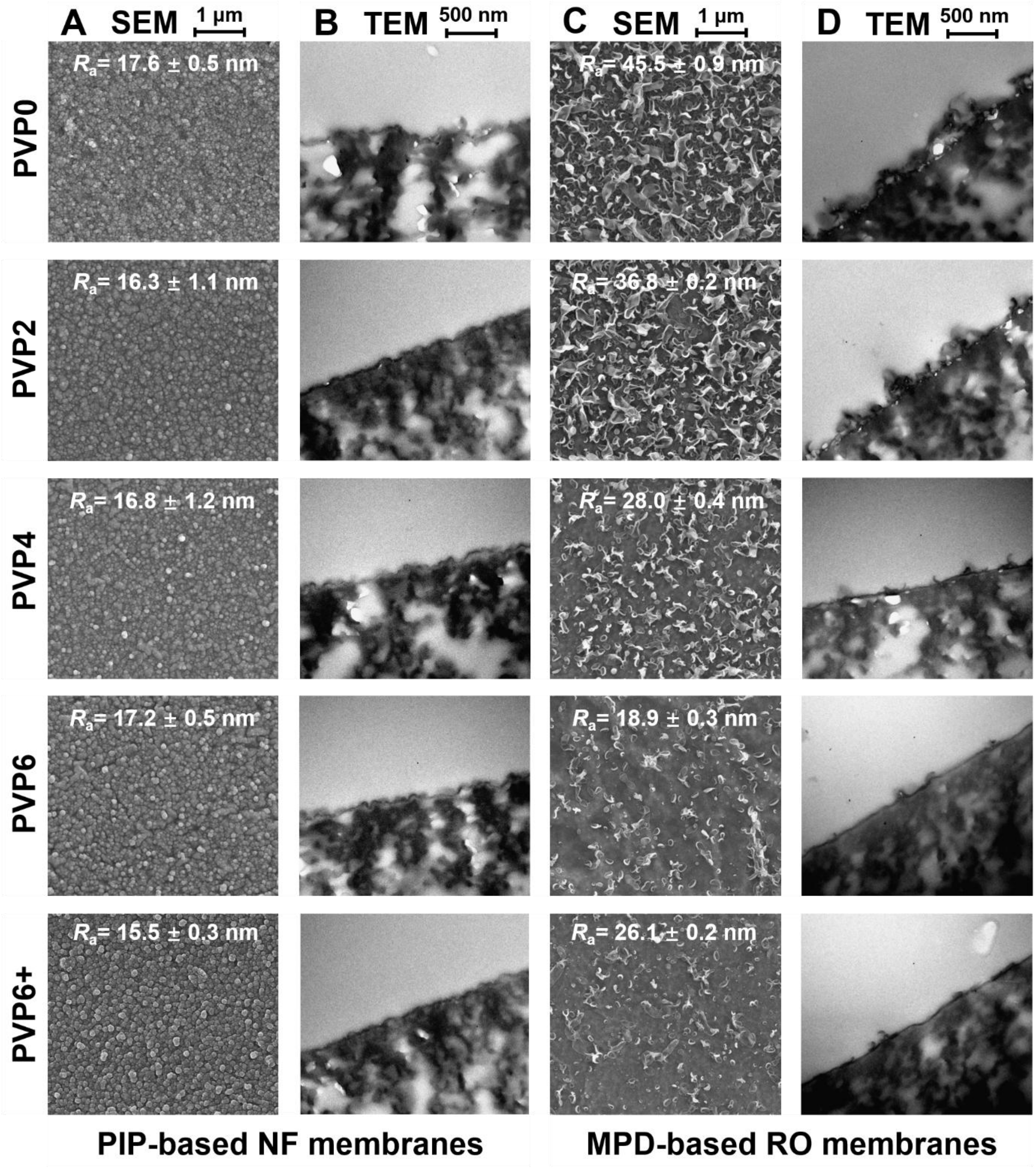

Fig. 3. Morphological characterization of surfaces and cross-sections of TFC membranes prepared on different PSf substrates. (A) SEM characterization of surfaces of NF membranes. (B) TEM characterization of cross-sections of NF membranes. (C) SEM characterization of surfaces of RO membranes. (D) TEM characterization of cross-sections of RO membranes. Prior to the SEM characterization, the surfaces of TFC membranes were subject to gold

sputtering for enhancing conductivity. Embedment and ultrathin sectioning were performed before TEM cross-sectional characterization of the TFC membranes. The R_a values shown in SEM images represent the surface roughness measured by AFM for different membranes.

Notably, amine concentration has been demonstrated to have a profound impact on the leaf-like PA structure of RO membranes[25,26]. It was reported that a more intensified leaf-like structure would be formed if the bulk MPD concentration increased[26], and reducing restrictions in the MPD supply can even allow secondary formation of leaf-like structure on the as-prepared NF/RO membranes[25]. In current study, constant MPD solution (2.0 wt/v%) was employed to wet the substrates with varied hydrophilicity. To deconvolute the possible difference in monomer-PSf interaction and water-PSf interaction, a molecular docking simulation experiment was conducted. The simulation indicates a stronger interaction of PIP with PSf for NF membranes (or MPD with PSf for RO membranes) compared to water-PSf (Fig. 4A). This result implied the different interaction condition of monomers and water to the PSf substrate. We further determined monomer/water uptake and monomer sorption by various substrates with different hydrophilicity. Both the sorption of PIP/water and MPD/water by substrates increased with the enhancement of substrate hydrophilicity[18,44] (Figs. 4B and 4C). However, interestingly, the sorption of PIP and MPD monomers alone by substrates kept nearly constant despite the change in the hydrophilicity (Figs. 4D and 4E). This contrasting sorption behaviors suggested that the concentration of monomers on the surface of hydrophilic substrate would be markedly lower (constant PIP or MPD divided by more adsorbed water) than that on the surface of hydrophobic substrate. In other words, the monomers of PIP and MPD were concentrated on the surface of hydrophobic substrates (Fig. S5), creating a local region with a higher concentration of monomers that reacted with TMC more dramatically during IP.

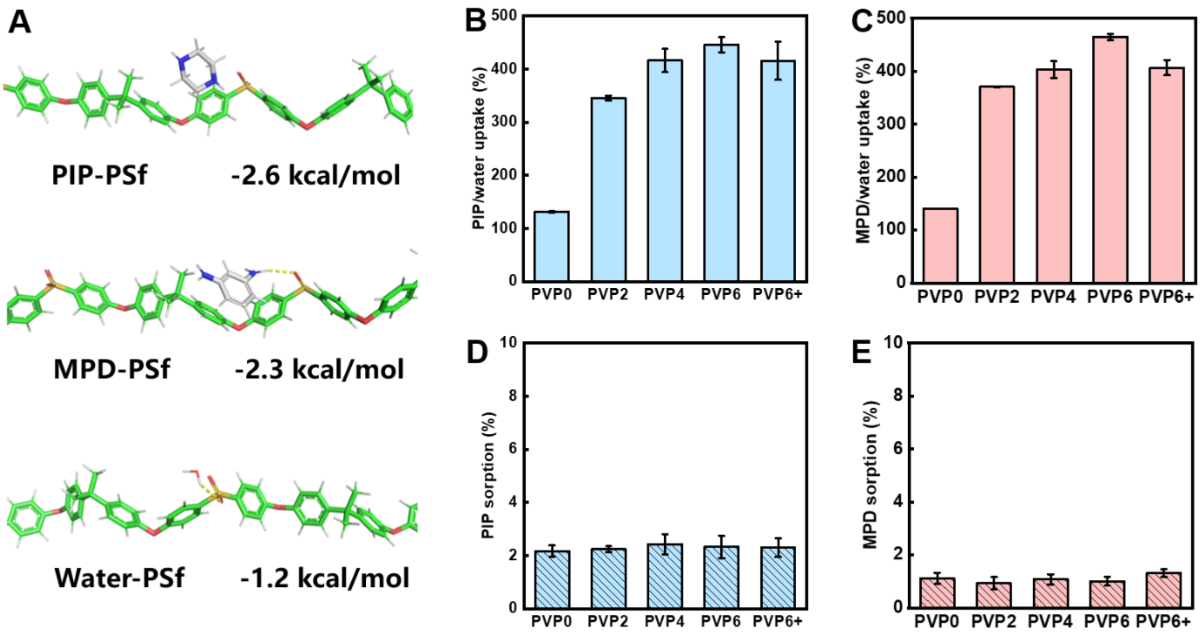

Fig. 4. The contrasting phenomenon in water and monomer uptakes for different PSf substrates with varied hydrophilicity. (A) Interaction forces between monomers-PSf and water-PSf calculated by a molecular docking simulation experiment. (B) PIP/water uptake of different substrates determined by weighting method; (C) MPD/water uptake of different substrates determined by weighting method; (D) PIP sorption of different substrates. (E) MPD sorption of different substrates. The substrates after PIP/water or MPD/water uptake test were dried and subject to XPS characterization for determining PIP or MPD sorption quantity.

The IP of diluted PIP/MPD and TMC monomers on relatively hydrophilic substrates (Fig. 5A) enabled a more thermodynamically unfavorable reaction, resulting in PA membranes with lower cross-linking degrees (Fig. 5B). Moreover, AFM scanning at the border of isolated PA layer and silicon wafer suggested that the PA apparent thicknesses of both NF and RO membranes on hydrophilic substrates were lower than those on relatively hydrophobic substrates (Fig. 5C, Figs. S6 and S7), which further validates the reduced IP rates for the hydrophilic substrates. The apparent thickness was used for normalizing the water permeance to obtain the apparent water permeability (Fig. S8). The nearly comparable apparent water permeabilities for NF membranes implies the critical impact of apparent thickness on the water permeance, while the marginal difference among the apparent water permeabilities should be ascribed to the influence of cross-linking degree. The looser and thinner PA structure benefits the increase in water permeance (Fig. 5D), as observed for the NF membranes. However, the RO membranes showed both substantially decreased water permeance and apparent water permeability after the substrate became more hydrophilic (Fig. 5D, Fig. S8), though the variation of the local monomer concentration, the cross-linking degree, and apparent thickness of RO membranes showed the same tendency as those of NF membranes (Figs. 5A-C). Importantly, the PA roughness of RO membrane was in positive correlation with the water contact angle of substrate (R^2=0.99, Fig. 5E) and the water permeance (R^2=0.81, Fig. 5F), which further highlighted the critical role of nanovoids that originated from interfacially degassed nanobubbles in RO performance[27].

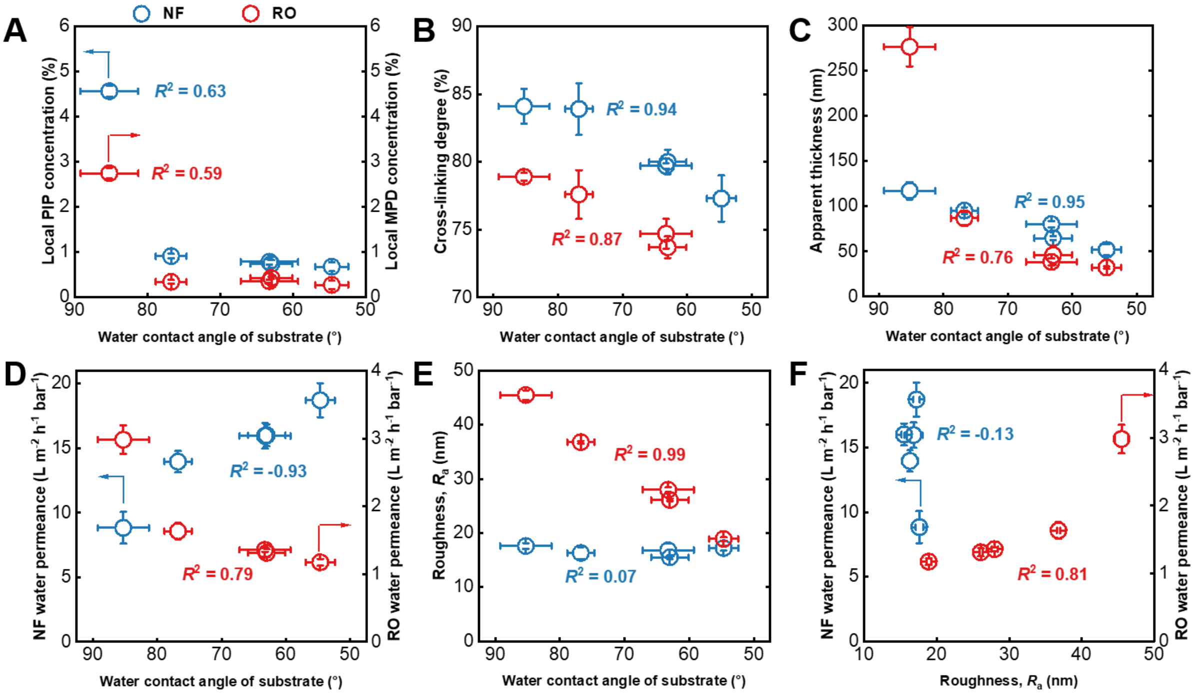

Fig. 5. Correlations between the water contact angle of substrate with the structure and water permeance of the TFC NF and RO membranes. (A) Water contact angles of substrates versus local monomer concentrations; (B) Water contact angles of substrates versus cross-linking degrees of PA layers; (C) Water contact angles of substrates versus apparent thicknesses of PA layers; (D) Water contact angles of substrates versus water permeances; (E) Water contact angles of substrates versus PA roughness; (F) PA roughness versus water permeances. R^2 in the figure, which was obtained from Microsoft Excel, represents the correlation coefficient between different parameters. The blue and red points correspond to data of the NF and RO membranes, respectively.

3.4. Mechanistic insights

In order to further reveal the mechanisms governing the impact of substrate hydrophilicity on structure and performance of PA layers, we prepared PA nanofilms at free interfaces for both PIP-TMC and MPD-TMC systems, which were further loaded on PVP0 and PVP6 substrates.

The lack of confinement effect at the free interface enables freely escaping of nanobubbles resulting from interfacial degassing[26,30], which would suppress the formation of nanovoids within PA nanofilms, especially for the RO membranes. The NF-fi membranes ("fi" represents TFC membranes fabricated at the free interface) still presented typical nodular structures (Fig. S9A) when the preparation conditions were changed from the direct IP to the free interface, which implied that the interfacial degassing mechanism did not play dominant role in the formation of nodular morphology of the NF membranes. In contrast, the leaf-like structure disappeared for both RO-fi-PVP0 and RO-fi-PVP6 membranes (Fig. S9B), highlighting the suppressed templating function of nanobubbles due to the loss of confinement effect[26,30].

The NF-fi-PVP0 membrane showed comparable water permeance to the one prepared from the direct IP (Fig. S10A), while the NF-fi-PVP6 membrane possessed markedly lower water permeance than the corresponding one of the direct IP. This phenomenon could be explained by the fact that the IP at free interface has sufficient supply of reactive monomers, which results in a more cross-linked PA nanofilm. Simultaneously, the water permeance of RO-fi-PVP0 membrane was significantly compromised (~ 1 L m^{-2} h^{-1} bar^{-1}) compared with that of the RO membrane prepared from the direct IP (Fig. S10B). This result further underlined that nanovoids in PA nanofilms of RO membranes strongly contributed to the water permeance of the whole membrane.

According to the nanobubble theory (or the interfacial degassing theory)[18,27,30], more available MPD monomer could induce a more intensive heat generation at the interface of IP reaction, which boosts the production of CO_2 nanobubbles and thereby intensifies the shaping effect [25–27]. Here, the more hydrophilic substrate with lower local MPD concentration on the surface leads to a weaker production of heat and thereby inhibited the release of CO_2 nanobubbles between substrates and PA nanofilms (Fig. 6). This reason was responsible for the diminished leaf-like structure of RO membranes when the substrates became more hydrophilic. Since the leaf-like structure was highly correlated with the effective surface area for water transport, the diminished leaf-like structure would cause a decrease in water permeance of RO membranes[14,15]. Although the cross-linking degree of the RO membrane decreased, the looser structure of the RO membrane could not compensate for the water permeance loss induced by the reduced effective surface area.

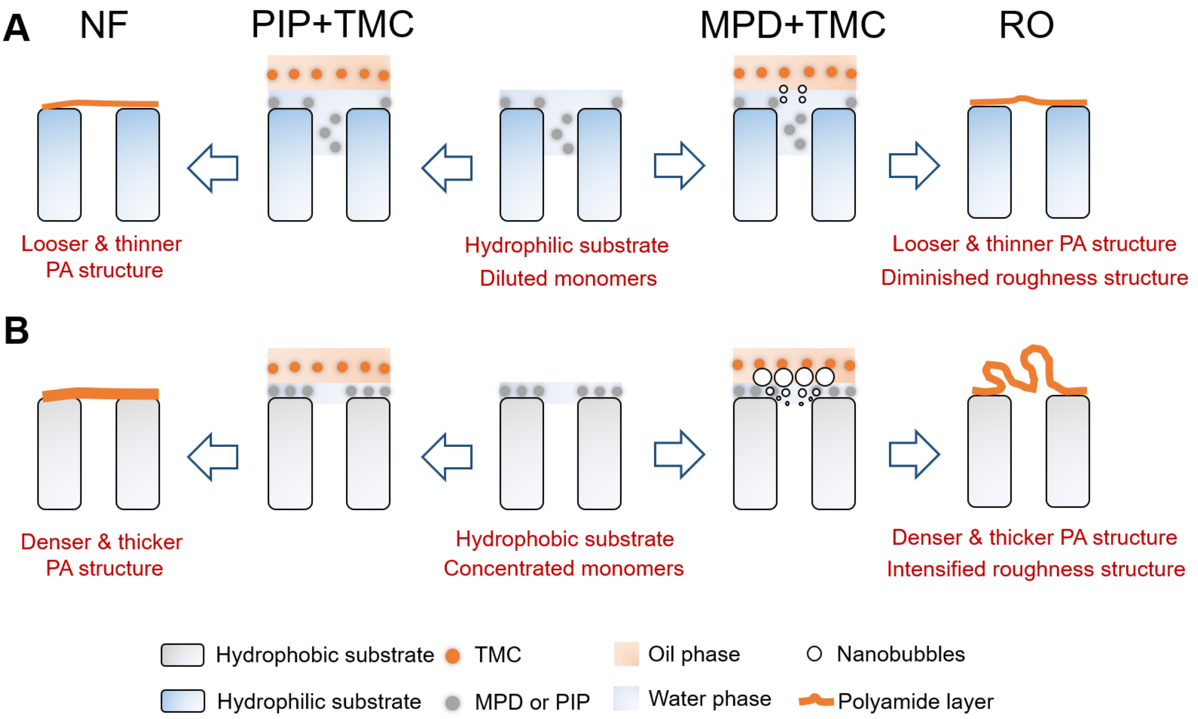

Fig. 6. Mechanistic illustration on the effects of hydrophilicity of substrates on the interfacial polymerization process and structure of NF and RO membranes. (A) Hydrophilic substrate; (B) Hydrophobic substrate.

Currently, the nanobubble theory was barely studied in the field of NF membrane.

Nevertheless, the nanobubble generated in the IP process of NF membrane should be, theoretically, less important due to the weaker reaction rate and lower heat generation of PIP-TMC reaction than that of MPD-TMC reaction[27,31,32]. Therefore, the more hydrophilic substrate with lower local PIP concentration resulted in the NF membrane with a looser and thinner PA layer, corresponding to the higher water permeance. One should note that the nanobubble theory in PIP-TMC system still requires further investigation to better elucidate why the potential nanobubbles can hardly shape the PA structure of the NF membrane.

3.5. Perspectives

TFC-PA NF and RO membranes are widely applied in wastewater treatment, water reuse and seawater desalination.[2,3] The current study revealed the distinct impact of substrates with different hydrophilicity on the performance and structure of TFC-PA NF and RO membranes. We highlighted the two fundamental mechanisms (locally concentrated aqueous monomers on hydrophobic surface and interfacial degassing) in the different responses of NF and RO membranes to the substrates. Generally, increased substrate hydrophilicity can lead to a weakened IP and thus a looser and thinner PA structure, due to the diluted monomer concentration (PIP/MPD) on the substrate. At the same time, the interfacial nanobubble generation was inhibited for the MPD-TMC system because of the weakened reaction and heat production, resulting in a decrease in the roughness feature and compromised water permeance of RO membranes. Since the interfacial degassing mechanism was not obvious in the PIP-TMC system due to the slower reaction rate of PIP-TMC compared to MPD-TMC, the performance and structure of NF membranes were mainly governed by the local monomer concentration with the exclusion of the interfacial degassing. Therefore, the water permeance of NF membrane was enhanced when the substrate became more hydrophilic, resulting from the looser and thinner PA structure.

Our study indicates that TFC-PA NF membranes favor more hydrophilic substrates while relatively hydrophobic substrates are more suitable for the fabrication of TFC-PA RO membranes. This principle can partially rationalize the phenomenon that hydrophilic interlayer modification on hydrophobic substrate often benefits the synthesis of high water permeance NF membranes[10,23,24]. The adverse impact of increased hydrophilicity of substrates on the performance of RO membranes, which is consistent with previous studies[19,40], suggests that relatively hydrophobic substrate or interlayer will be possibly effective in further optimizing the structure and enhancing the performance of RO membranes. Nevertheless, one should note that highly hydrophobic substrates such as polyvinylidene[45,46] or polypropylene substrates[47,48] with water contact angles greater than 100° would not be suitable for high performance RO membrane fabrication due to the substantially limited water sorption on the substrates, and ultra-hydrophilic substrates like polyacrylonitrile with a water contact angle <40° could induce the delamination of the PA layer[49]. The critical points of hydrophobic and hydrophilic substrates for ideal RO and NF membranes should be explored in future studies, respectively, which can facilitate the development of customized membrane for efficient water and wastewater treatment.

It should be noted that the pore size of different substrates in this study still showed slight difference, which may also contribute to the change in structure and performance of TFC-PA NF and RO membranes. Creating substrates that have strictly the same pore size with different hydrophilicity is needed for future studies. In addition, for identical PA layers, substrates with higher hydrophilicity could somewhat facilitate water transport and thereby improve the water permeance of the whole TFC membranes. Although this phenomenon is neglectable in this study (as demonstrated in the free interface experiment of Figs. S9 and S10), this effect should be taken into consideration in future experimental design.

4. Conclusions

The TFC RO membrane showed higher water permeance and NaCl rejection on the relatively hydrophobic substrate, while the TFC NF membrane favored the relatively hydrophilic substrate. We highlighted the critical importance of interfacial degassing and local monomer concentration to dissect the distinct impact of substrate hydrophilicity. For the MPD-TMC system, interfacial nanobubble generation was inhibited because of the decreased local MPD concentration and heat production for the more hydrophilic substrates, resulting in a decrease in the roughness feature and compromised water permeance of RO membranes. In contrast, interfacial degassing was not a dominant mechanism in the PIP-TMC system due to the slower reaction rate of PIP-TMC than MPD-TMC. The PA layer of NF membrane hence became thinner and looser when the substrate was more hydrophilic, resulting from the diluted local PIP concentration.

CRediT authorship contribution statement

Ruobin Dai: Conceptualization, Methodology, Investigation, Formal analysis, Writing – original draft. **Zhe Yang:** Conceptualization, Methodology, Investigation. **Zhiwei Qiu:**

Methodology, Investigation. **Li Long:** Methodology, Investigation. **Chuyang Y. Tang:** Supervision, Project administration, Formal analysis, Writing – review & editing, Funding acquisition. **Zhiwei Wang:** Supervision, Project administration, Formal analysis, Writing – review & editing, Funding acquisition.

Declaration of competing interest

The authors declare that they have no known competing financial interests or personal relationships that could have appeared to influence the work reported in this paper.

Data availability

Data will be made available on request.

Acknowledgements

We thank the National Key Research and Development Program of China (2019YFC0408200), the National Natural Science Foundation of China (51925806), and the Shanghai Sailing Program (22YF1450700) for the financial support of the work. CYT is supported by the Senior Research Fellow Scheme of the Research Grants Council of the Hong Kong Special Administrative Region, China (SRFS2021-7S04).

Appendix A. Supplementary data

Supplementary data to this article can be found online at …

References

[1] H.B. Park, J. Kamcev, L.M. Robeson, M. Elimelech, B.D. Freeman, Maximizing the right stuff: The trade-off between membrane permeability and selectivity, Science. 356 (2017) eaab0530. https://doi.org/10.1126/science.aab0530.

[2] B.E. Logan, M. Elimelech, Membrane-based processes for sustainable power generation using water, Nature. 488 (2012) 313–319. https://doi.org/10.1038/nature11477.

[3] H. Guo, R. Dai, M. Xie, L.E. Peng, Z. Yao, Z. Yang, L.D. Nghiem, S.A. Snyder, Z. Wang, C.Y. Tang, Tweak in Puzzle: Tailoring Membrane Chemistry and Structure toward Targeted Removal of Organic Micropollutants for Water Reuse, Environmental Science & Technology Letters. 9 (2022) 247–257. https://doi.org/10.1021/acs.estlett.2c00094.

[4] M.A. Shannon, P.W. Bohn, M. Elimelech, J.G. Georgiadis, B.J. Mariñas, A.M. Mayes, Science and technology for water purification in the coming decades, Nature. 452 (2008) 301–310. https://doi.org/10.1038/nature06599.

[5] M. Elimelech, W.A. Phillip, The Future of Seawater Desalination: Energy, Technology, and the Environment, Science. 333 (2011) 712–717. https://doi.org/10.1126/science.1200488.

[6] A. Anantharaman, Y. Chun, T. Hua, J.W. Chew, R. Wang, Pre-deposited dynamic membrane filtration – A review, Water Research. 173 (2020) 115558. https://doi.org/10.1016/j.watres.2020.115558.

[7] Z. Tan, S. Chen, X. Peng, L. Zhang, C. Gao, Polyamide membranes with nanoscale Turing structures for water purification, Science. 360 (2018) 518–521. https://doi.org/10.1126/science.aar6308.

[8] B. Sapkota, W. Liang, A. VahidMohammadi, R. Karnik, A. Noy, M. Wanunu, High permeability sub-nanometre sieve composite MoS 2 membranes, Nature Communications. 11 (2020) 2747. https://doi.org/10.1038/s41467-020-16577-y.

[9] Y. Wen, R. Dai, X. Li, X. Zhang, X. Cao, Z. Wu, S. Lin, C.Y. Tang, Z. Wang, Metal-organic framework enables ultraselective polyamide membrane for desalination and water reuse, Science Advances. 8 (2022) eabm4149. https://doi.org/10.1126/sciadv.abm4149.

[10] R. Dai, J. Li, Z. Wang, Constructing interlayer to tailor structure and performance of thin-film composite polyamide membranes: A review, Advances in Colloid and Interface Science. 282 (2020) 102204. https://doi.org/10.1016/j.cis.2020.102204.

[11] X. Lu, M. Elimelech, Fabrication of desalination membranes by interfacial polymerization: history, current efforts, and future directions, Chemical Society Reviews. 50 (2021) 6290–6307. https://doi.org/10.1039/D0CS00502A.

[12] Y. Cui, X.-Y. Liu, T.-S. Chung, Ultrathin Polyamide Membranes Fabricated from Free-Standing Interfacial Polymerization: Synthesis, Modifications, and Post-treatment, Industrial & Engineering Chemistry Research. 56 (2017) 513–523. https://doi.org/10.1021/acs.iecr.6b04283.

[13] B. Yuan, S. Zhao, P. Hu, J. Cui, Q.J. Niu, Asymmetric polyamide nanofilms with highly ordered nanovoids for water purification, Nature Communications. 11 (2020) 6102. https://doi.org/10.1038/s41467-020-19809-3.

[14] X. Song, B. Gan, S. Qi, H. Guo, C.Y. Tang, Y. Zhou, C. Gao, Intrinsic Nanoscale Structure of Thin Film Composite Polyamide Membranes: Connectivity, Defects, and Structure–

Property Correlation, Environ. Sci. Technol. 54 (2020) 3559–3569. https://doi.org/10.1021/acs.est.9b05892.

[15] L. Lin, R. Lopez, G.Z. Ramon, O. Coronell, Investigating the void structure of the polyamide active layers of thin-film composite membranes, Journal of Membrane Science. 497 (2016) 365–376. https://doi.org/10.1016/j.memsci.2015.09.020.

[16] L. Shen, R. Cheng, M. Yi, W.-S. Hung, S. Japip, L. Tian, X. Zhang, S. Jiang, S. Li, Y. Wang, Polyamide-based membranes with structural homogeneity for ultrafast molecular sieving, Nat Commun. 13 (2022) 500. https://doi.org/10.1038/s41467-022-28183-1.

[17] L.E. Peng, Z. Yang, L. Long, S. Zhou, H. Guo, C.Y. Tang, A critical review on porous substrates of TFC polyamide membranes: Mechanisms, membrane performances, and future perspectives, Journal of Membrane Science. 641 (2022) 119871. https://doi.org/10.1016/j.memsci.2021.119871.

[18] L.E. Peng, Z. Yao, Z. Yang, H. Guo, C.Y. Tang, Dissecting the Role of Substrate on the Morphology and Separation Properties of Thin Film Composite Polyamide Membranes: Seeing Is Believing, Environ. Sci. Technol. 54 (2020) 6978–6986. https://doi.org/10.1021/acs.est.0c01427.

[19] A.K. Ghosh, E.M.V. Hoek, Impacts of support membrane structure and chemistry on polyamide–polysulfone interfacial composite membranes, Journal of Membrane Science. 336 (2009) 140–148. https://doi.org/10.1016/j.memsci.2009.03.024.

[20] Z. Yali, L.G. Sung, W. Yining, L. Can, W. Rong, Impact of pilot-scale PSF substrate surface and pore structural properties on tailoring seawater reverse osmosis membrane performance, Journal of Membrane Science. 633 (2021) 119395. https://doi.org/10.1016/j.memsci.2021.119395.

[21] X. Li, Q. Li, W. Fang, R. Wang, W.B. Krantz, Effects of the support on the characteristics and permselectivity of thin film composite membranes, Journal of Membrane Science. 580 (2019) 12–23. https://doi.org/10.1016/j.memsci.2019.03.003.

[22] M.F. Jimenez-Solomon, P. Gorgojo, M. Munoz-Ibanez, A.G. Livingston, Beneath the surface: Influence of supports on thin film composite membranes by interfacial polymerization for organic solvent nanofiltration, Journal of Membrane Science. 448 (2013) 102–113. https://doi.org/10.1016/j.memsci.2013.06.030.

[23] Z. Yang, F. Wang, H. Guo, L.E. Peng, X. Ma, X. Song, Z. Wang, C.Y. Tang, Mechanistic Insights into the Role of Polydopamine Interlayer toward Improved Separation Performance of Polyamide Nanofiltration Membranes, Environ. Sci. Technol. 54 (2020) 11611–11621. https://doi.org/10.1021/acs.est.0c03589.

[24] Z. Yang, Z. Zhou, H. Guo, Z. Yao, X. Ma, X. Song, S.-P. Feng, C.Y. Tang, Tannic Acid/Fe $^{3+}$ Nanoscaffold for Interfacial Polymerization: Toward Enhanced Nanofiltration Performance, Environmental Science & Technology. 52 (2018) 9341–9349. https://doi.org/10.1021/acs.est.8b02425.

[25] K. Grzebyk, M.D. Armstrong, O. Coronell, Accessing greater thickness and new morphology features in polyamide active layers of thin-film composite membranes by reducing restrictions in amine monomer supply, Journal of Membrane Science. 644 (2022) 120112. https://doi.org/10.1016/j.memsci.2021.120112.

[26] L.E. Peng, Q. Gan, Z. Yang, L. Wang, P.-F. Sun, H. Guo, H.-D. Park, C.Y. Tang, Deciphering the Role of Amine Concentration on Polyamide Formation toward Enhanced

RO Performance, ACS EST Eng. (2022) acsestengg.1c00418. https://doi.org/10.1021/acsestengg.1c00418.

[27] X.-H. Ma, Z.-K. Yao, Z. Yang, H. Guo, Z.-L. Xu, C.Y. Tang, M. Elimelech, Nanofoaming of Polyamide Desalination Membranes To Tune Permeability and Selectivity, Environmental Science & Technology Letters. 5 (2018) 123–130. https://doi.org/10.1021/acs.estlett.8b00016.

[28] X. Ma, Z. Yang, Z. Yao, H. Guo, Z. Xu, C.Y. Tang, Tuning roughness features of thin film composite polyamide membranes for simultaneously enhanced permeability, selectivity and anti-fouling performance, Journal of Colloid and Interface Science. 540 (2019) 382–388. https://doi.org/10.1016/j.jcis.2019.01.033.

[29] L.E. Peng, Z. Yao, X. Liu, B. Deng, H. Guo, C.Y. Tang, Tailoring Polyamide Rejection Layer with Aqueous Carbonate Chemistry for Enhanced Membrane Separation: Mechanistic Insights, Chemistry-Structure-Property Relationship, and Environmental Implications, Environ. Sci. Technol. 53 (2019) 9764–9770. https://doi.org/10.1021/acs.est.9b03210.

[30] X. Song, B. Gan, Z. Yang, C.Y. Tang, C. Gao, Confined nanobubbles shape the surface roughness structures of thin film composite polyamide desalination membranes, Journal of Membrane Science. 582 (2019) 342–349. https://doi.org/10.1016/j.memsci.2019.04.027.

[31] B. Ukrainsky, G.Z. Ramon, Temperature measurement of the reaction zone during polyamide film formation by interfacial polymerization, Journal of Membrane Science. 566 (2018) 329–335. https://doi.org/10.1016/j.memsci.2018.09.011.

[32] V. Freger, Nanoscale Heterogeneity of Polyamide Membranes Formed by Interfacial Polymerization, Langmuir. 19 (2003) 4791–4797. https://doi.org/10.1021/la020920q.

[33] Z. Yang, Y. Wu, J. Wang, B. Cao, C.Y. Tang, In Situ Reduction of Silver by Polydopamine: A Novel Antimicrobial Modification of a Thin-Film Composite Polyamide Membrane, Environ. Sci. Technol. 50 (2016) 9543–9550. https://doi.org/10.1021/acs.est.6b01867.

[34] R. Dai, X. Zhang, M. Liu, Z. Wu, Z. Wang, Porous metal organic framework CuBDC nanosheet incorporated thin-film nanocomposite membrane for high-performance forward osmosis, Journal of Membrane Science. 573 (2019) 46–54. https://doi.org/10.1016/j.memsci.2018.11.075.

[35] R. Dai, H. Guo, C.Y. Tang, M. Chen, J. Li, Z. Wang, Hydrophilic Selective Nanochannels Created by Metal Organic Frameworks in Nanofiltration Membranes Enhance Rejection of Hydrophobic Endocrine-Disrupting Compounds, Environmental Science & Technology. 53 (2019) 13776–13783. https://doi.org/10.1021/acs.est.9b05343.

[36] A.G. Fane, C. Tang, R. Wang, Membrane technology for water: microfiltration, ultrafiltration, nanofiltration, and reverse osmosis, Treatise on Water Science 4. (2011).

[37] W.A.W. Rafizah, A.F. Ismail, Effect of carbon molecular sieve sizing with poly(vinyl pyrrolidone) K-15 on carbon molecular sieve–polysulfone mixed matrix membrane, Journal of Membrane Science. 307 (2008) 53–61. https://doi.org/10.1016/j.memsci.2007.09.007.

[38] S. Koga, T. Yakushiji, M. Matsuda, K. Yamamoto, K. Sakai, Functional-group analysis of polyvinylpyrrolidone on the inner surface of hollow-fiber dialysis membranes, by near-field infrared microspectroscopy, Journal of Membrane Science. 355 (2010) 208–213.

https://doi.org/10.1016/j.memsci.2010.03.032.

[39] T. Xiang, W.-W. Yue, R. Wang, S. Liang, S.-D. Sun, C.-S. Zhao, Surface hydrophilic modification of polyethersulfone membranes by surface-initiated ATRP with enhanced blood compatibility, Colloids and Surfaces B: Biointerfaces. 110 (2013) 15–21. https://doi.org/10.1016/j.colsurfb.2013.04.034.

[40] B. Deng, Effects of Polysulfone (PSf) Support Layer on the Performance of Thin-Film Composite (TFC) Membranes, Journal of Chemical and Process Engineering. (2013). https://doi.org/10.17303/jce.2014.102.

[41] L.D. Nghiem, A.I. Schäfer, M. Elimelech, Removal of Natural Hormones by Nanofiltration Membranes: Measurement, Modeling, and Mechanisms, Environmental Science & Technology. 38 (2004) 1888–1896. https://doi.org/10.1021/es034952r.

[42] N. Akther, S. Phuntsho, Y. Chen, N. Ghaffour, H.K. Shon, Recent advances in nanomaterial-modified polyamide thin-film composite membranes for forward osmosis processes, Journal of Membrane Science. 584 (2019) 20–45. https://doi.org/10.1016/j.memsci.2019.04.064.

[43] M.R. Chowdhury, J. Steffes, B.D. Huey, J.R. McCutcheon, 3D printed polyamide membranes for desalination, Science. 361 (2018) 682–686. https://doi.org/10.1126/science.aar2122.

[44] R. Dai, H. Han, T. Wang, J. Li, Z. Wu, C.Y. Tang, Z. Wang, Cleaning–Healing–Interfacial Polymerization Strategy for Upcycling Real End-of-Life Polyvinylidene Fluoride Microfiltration Membranes, ACS Sustainable Chem. Eng. 9 (2021) 10352–10360. https://doi.org/10.1021/acssuschemeng.1c03481.

[45] X. Zhang, L. Shen, W.-Z. Lang, Y. Wang, Improved performance of thin-film composite membrane with PVDF/PFSA substrate for forward osmosis process, Journal of Membrane Science. 535 (2017) 188–199. https://doi.org/10.1016/j.memsci.2017.04.038.

[46] H.-M. Cui, X. Yan, Y. Chen, W.-Y. Xu, W.-Z. Lang, Enhanced performance of forward osmosis membranes by incorporating PVDF substrates with hydrophilic nanofillers, DWT. 155 (2019) 1–14. https://doi.org/10.5004/dwt.2019.23868.

[47] H.I. Kim, S.S. Kim, Plasma treatment of polypropylene and polysulfone supports for thin film composite reverse osmosis membrane, Journal of Membrane Science. 286 (2006) 193–201. https://doi.org/10.1016/j.memsci.2006.09.037.

[48] K. Pan, H. Gu, B. Cao, Interfacially polymerized thin-film composite membrane on UV-induced surface hydrophilic-modified polypropylene support for nanofiltration, Polym. Bull. 71 (2014) 415–431. https://doi.org/10.1007/s00289-013-1068-z.

[49] X. Liu, G. Liu, W. Li, Q. Wang, B. Deng, Effects of the Substrate on Interfacial Polymerization: Tuning the Hydrophobicity via Polyelectrolyte Deposition, Membranes. 10 (2020) 259. https://doi.org/10.3390/membranes10100259.